



Synthesis of Freestanding Graphene on SiC by a Rapid-Cooling Technique

Jianfeng Bao,^{1,†} Wataru Norimatsu,^{2,*} Hiroshi Iwata,² Keita Matsuda,² Takahiro Ito,³ and Michiko Kusunoki¹

¹*Institute of Materials and Systems for Sustainability, Nagoya University, Nagoya 464-8603, Japan*

²*Department of Applied Chemistry, Graduate School of Engineering, Nagoya University, Nagoya 464-8603, Japan*

³*Synchrotron Radiation Research Center, Nagoya University, Nagoya 464-8603, Japan*

(Received 15 April 2016; revised manuscript received 8 July 2016; published 8 November 2016)

Graphene has a negative thermal expansion coefficient; that is, when heated, the graphene lattice shrinks. On the other hand, the substrates typically used for graphene growth, such as silicon carbide, have a positive thermal expansion coefficient. Hence, on cooling graphene on SiC, graphene expands but SiC shrinks. This mismatch will physically break the atomic bonds between graphene and SiC. We have demonstrated that a graphenelike buffer layer on SiC can be converted to a quasifreestanding monolayer graphene by a rapid-cooling treatment. The decoupling of graphene from the SiC substrate was actually effective for reducing the electric carrier scattering due to interfacial phonons. In addition, the rapidly cooled graphene obtained in this way was of high-quality, strain-free, thermally stable, and strongly hole doped. This simple, classical, but quite novel technique for obtaining quasifreestanding graphene could open a new path towards a viable graphene-based semiconductor industry.

DOI: 10.1103/PhysRevLett.117.205501

Graphene, a one atom thick two-dimensional crystal, has been considered as one of the promising candidate materials for the new generation of electronic devices because of its unique properties [1–3]. Among the several synthesis approaches employed, thermal decomposition of SiC is the most promising technique for high quality, transfer-free, and wafer-scale graphene production [4–6]. However, the carrier mobility in epitaxial monolayer graphene (EMLG) on SiC at room temperature is reduced compared to that at low temperatures due to the carrier scattering by phonons in the buffer layer [7]. The buffer layer is present between graphene and the SiC surface, and has a graphenelike honeycomb structure with covalent bonds to the Si atoms of SiC and with the $6\sqrt{3} \times 6\sqrt{3}R30$ ($6\sqrt{3}$) reconstructed structure [8,9]. It does not exhibit a graphene π band and is electrically inactive [10]. Thus, buffer layer elimination is key for reducing the phonon scattering. The most popular technique for buffer layer elimination is hydrogen intercalation in the interface [11]. In this way, the buffer layer can be converted to monolayer graphene, and then it is referred to as quasifreestanding monolayer graphene (QFSMLG) [11,12]. In this Letter, we report on a novel technique for obtaining thermally stable QFSMLG without using explosive hydrogen gas, which has the advantage of greatly reducing the safety measures required.

In order to obtain QFSMLG, we focused on the fact that graphene has a negative thermal expansion coefficient (TEC) [13–16]. Figure 1(a) shows the temperature dependence of the lattice parameter a in graphene and $6H$ -SiC [13,17]. The TEC in graphene is negative up to about 973 K and then changes sign at higher temperatures, but the a value at 1273 K is still lower than that at 50 K. We then anticipated that if we rapidly cooled the graphenelike buffer layer on

SiC, the buffer layer would expand but the SiC would shrink, leading to the physical breaking of the bonds between them as illustrated in Fig. 1(b). We here assumed that the TEC of the buffer layer was also negative, because the in-plane structure of the buffer layer and graphene is almost the same [8]. In this study, we demonstrate that the rapid cooling (RC) treatment actually converts the buffer layer into QFSMLG, which was homogeneous with p -type conduction and without the phonon scattering due to the buffer layer, and it was also free from strain and was thermally stable.

We prepared the buffer layer sample, which was homogeneous over an area of 5×5 mm². [18] The RC process includes heating the buffer layer sample to more than 1073 K, followed by rapid cooling to 77 K by dropping it directly into liquid nitrogen [18]. In order to avoid oxidation during heating, the sample was vacuum sealed in a quartz tube.

We first checked the actual effect of the RC treatment by observing the interface directly using a high-resolution transmission electron microscope (HRTEM). Here we used multilayer graphene with 5–10 layers in order to easily visualize the RC effect. Figure 1(c) shows the results of the RC treatment. The initial graphene layers were directly attached to the SiC, while after the RC treatment from 1073 K, graphene layers detached from the substrate in some areas. This detachment was never observed in the as-grown graphene layers on SiC (0001) [8,19–21]. Based on our further experiments, we concluded that the optimum temperature for the RC treatment was around 1173 K [18]. In addition, interestingly, the samples cooled from more than 1073 K exhibited a p -type conduction, but the other samples, including the initial one, had an n -type conduction according to our Hall-effect measurements [18]. These

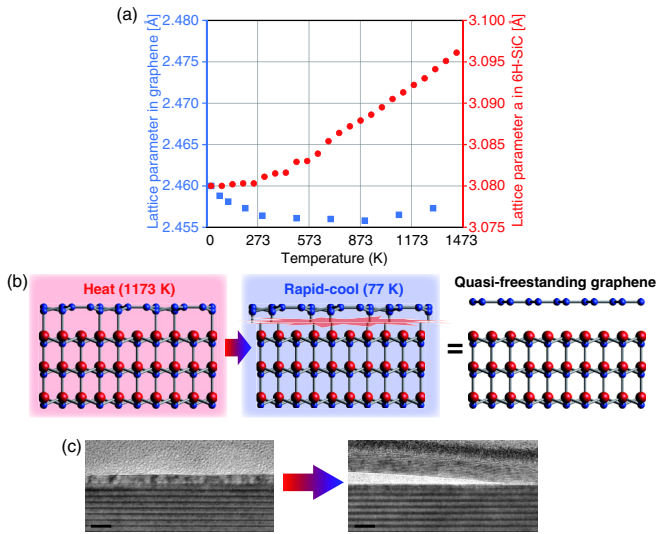


FIG. 1. (a) Temperature dependence of the lattice parameter a of graphene (squares, left axis) and $6H$ -SiC (circles, right axis). (b) Schematic diagram of the conversion of the buffer layer into QFSMLG by the RC treatment. In the left structure, the buffer layer on SiC is shown. The blue and red balls correspond to the carbon and silicon atoms, respectively. (c) HRTEM images of multilayer graphene samples before and after the RC treatment from 1073 to 77 K. The scale bar in the images is 5 nm.

results indicated that the RC treatment from higher than 1073 K induced a significant change in the interface of graphene with SiC.

We then used the homogeneous buffer layer sample [18]. The samples were rapidly cooled from 1173 to 77 K. Figure 2 shows atomic force microscope (AFM) images, Raman spectra, and the reflection high-energy electron diffraction (RHEED) results of the samples before and after the RC treatment. Raman spectra in this study are substrate corrected by subtracting a signal from a clean SiC surface. In Fig. 2(a), an atomically flat surface was observed. The AFM phase image has the major areas (95%) as bright and the minor (5%) as dark contrast. The contrast of the phase image is due to the difference in physical properties of the material. In the present case, the SiC surface is the darkest, and the thicker graphene has brighter contrast [8,21]. In the Raman spectra in Fig. 2(c), there are broad peaks at about 1350 and 1585 cm^{-1} . These peaks are the signature of the buffer layer [22]. The same features were observed at 30 different positions of this sample. These results indicated that about 95% of the surface of this sample was covered by the buffer layer, and the remaining 5% was the bare SiC surface.

After the RC treatment, the topographic features remained almost the same, as shown in Fig. 2(b). However, the Raman spectrum was completely different, as shown in Fig. 2(d). Instead of the broad peaks observed in the buffer layer, sharp peaks were clearly observed at 1595 and 2687 cm^{-1} . These peaks are known as the G and $2D$ bands, respectively, and are actually the evidence for the existence of graphene [23]. The

$2D$ peak could be fitted by a single Lorentzian with a full width at half maximum of 42.1 cm^{-1} , and the intensity of the $2D$ band is stronger than that of the G band, indicating the presence of monolayer graphene [24–26]. The same peaks were detected at 27 different positions on this sample. Corresponding results were also obtained by the RHEED experiments, which are shown in Figs. 2(e) and 2(f). Before RC, the diffraction streaks and spots due to the buffer layer which have $6\sqrt{3}$ structure were clearly observed along the arc shown by green arrows, in addition to the diffraction from SiC (blue arrows). After RC, these $6\sqrt{3}$ spots completely disappeared and the diffraction streaks due to graphene can be observed as shown by red arrows. Thus, we concluded that the buffer layer was converted to monolayer graphene. We performed the same RC experiment using some other samples, and found that in a sample containing both the buffer layer and EMLG, they were converted to monolayer and bilayer graphene, respectively [18].

In these experiments, the cooling rate is very important. Although it is difficult to precisely measure it, we roughly estimated that the sample was cooled from 1173 to 77 K in just a few seconds, considering the heat capacities and

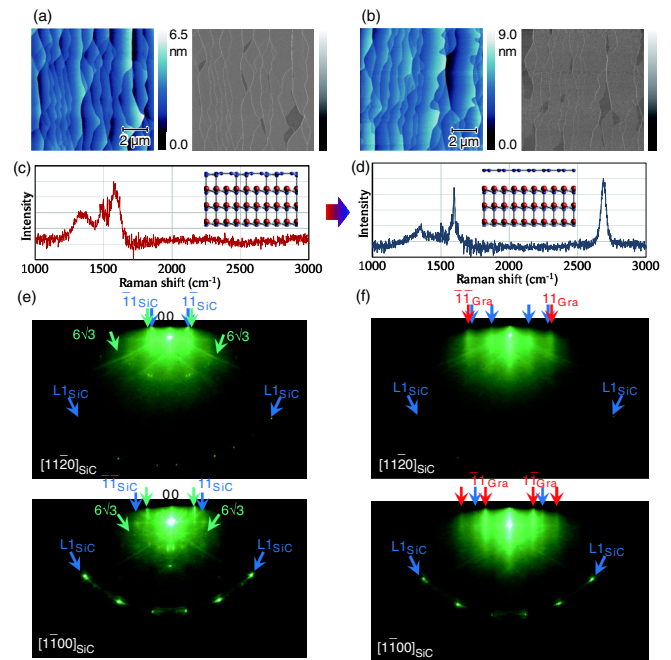


FIG. 2. The AFM topography and phase images of (a) before and (b) after the RC treatment. The bright areas in (a) and (b) correspond to the buffer layer and RCG, and the dark areas correspond to the bare SiC surface. The Raman spectra of (c) before and (d) after the RC treatment. Typical size of the laser spot was about 1 μm . The RHEED patterns of (e) before and (f) after rapid cooling are also shown. The diffraction spots and streaks due to SiC, the buffer layer, and graphene are denoted by blue, green, and red arrows, respectively. $L1_{\text{SiC}}$ spots indicate the diffraction spots of SiC in the first order Laue zone. Diffraction spots due to $6\sqrt{3}$ buffer layer can be seen along the arc shown by green arrows.

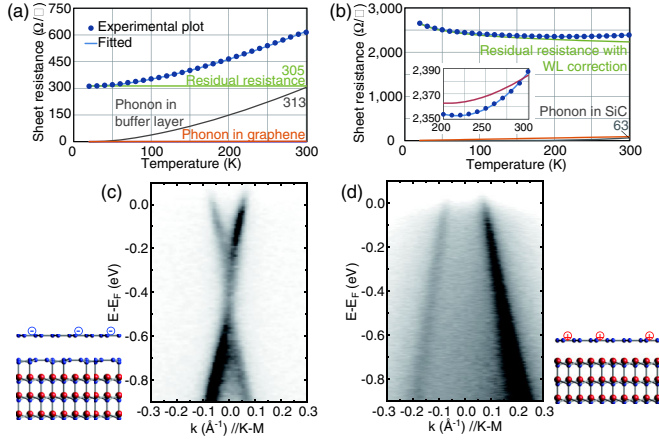


FIG. 3. Temperature dependence of the sheet resistance of (a) EMLG and (b) RCG. EMLG was grown at 1973 K in an Ar atmosphere. The plots are the experimental values and the blue lines indicate the theoretical fitting, together with the contribution of each component. The inset in (b) is the enlargement of the high temperature region, and the red and blue curves in it correspond to the best fits using the phonon energies of the buffer layer and SiC, respectively. ARPES spectra around the K point of (c) EMLG and (d) RCG, together with the schematic diagram of the corresponding atomic structure. The intensity of the band was asymmetric about the K point because the horizontal axis is along the K - M - K' line in reciprocal space.

thermal conductivities of the quartz tube and the SiC substrate. In order to confirm the effect of the RC treatment, we carried out the following control experiments. We heated the buffer layer sample to 1273 K, and then slowly cooled it down to 77 K within 10–20 sec. The Raman spectra in this experiment showed no changes before and after cooling [18]. These results clearly demonstrate that a very fast cooling rate is necessary for decoupling the buffer layer.

One of the significant features of the rapidly cooled graphene (RCG) is the position of the $2D$ band in the Raman spectrum. The typical EMLG has the $2D$ band at 2710 – 2730 cm^{-1} [24–26], and graphene exfoliated from a graphite crystal has the $2D$ band at about 2670 cm^{-1} . [23] This difference is due to the fact that the EMLG has a compressive strain due to the different TECs of graphene and SiC [24,26]. The RCG in Fig. 2(d) had a $2D$ band at 2687 cm^{-1} . We measured the Raman spectra at more than 100 positions in several RCG samples, and found that all $2D$ peaks were located between 2625 – 2695 cm^{-1} , and their positions are rather similar to strain-free graphene. These facts indicate that RCG is free from compressive strain. In other words, the RC process was the trigger to release graphene from strain due to the substrate.

We next investigated the electronic properties and structures of RCG, and compared them to typical EMLG. Figure 3 shows the temperature dependence of the electrical resistance and the electronic band structure around the K point in reciprocal space. The resistance of

EMLG increased with increasing temperature. The resistance of graphene obeys the following equation, according to Matthiessen's rule [27–30].

$$R = R_0 + R_{\text{LAP}} + R_{\text{IP}},$$

where R_0 , R_{LAP} , and R_{IP} are the residual resistance due to defects and impurities (which is not temperature dependent), the longitudinal acoustic phonon scattering of graphene, and interfacial phonon scattering term, respectively. Further,

$$R_{\text{LAP}} = \frac{\pi D_A^2 k_B}{e^2 \hbar \rho_s v_s^2 v_F^2} T.$$

Details of parameters and constants D_A , k_B , e , \hbar , ρ_s , v_s , and v_F are described in the Supplemental Material [18,27]. And,

$$R_{\text{IP}} = \sum_{i=1}^3 \left\{ \frac{C_i}{\exp[E_i/(k_B T)] - 1} \right\},$$

where C_i is the coefficient of the electron-phonon couplings, and E_i is the corresponding phonon energy. We used $E_1 = 70$, $E_2 = 16$, and $E_3 = 116$ meV, corresponding to the phonon energies of the buffer layer for E_1 and E_2 and the SiC surface for E_3 , respectively [28–30]. In the case of RCG, R_0 was converted to R_{WL} , which includes the weak localization correction,

$$R_{\text{WL}} = \frac{R_0}{1 + \frac{\alpha e^2 R_0}{2\pi^2 \hbar t} p \ln\left(\frac{T}{T_0}\right)}.$$

Details of α , p , t , and T_0 values are described in the Supplemental Material [18,31,32].

The resistance of EMLG was fitted by the parameters shown in Table I. The experimental plots were fitted quite well using these parameters. Here, phonon scattering in graphene was negligible. Figure 3(a) also shows the contribution of each component. At 20 K, the phonon scattering was negligible and the main contribution is the residual resistance. With increasing temperature, the contribution of the interfacial phonon scattering increased. The plots of EMLG could be fitted using only C_1 and C_2 , reflecting the fact that graphene lies on a buffer layer, not directly on SiC. At room temperature, more than half of the resistance is due to the interfacial phonon scattering.

In contrast, the resistance of RCG had the significantly different temperature dependence shown in Fig. 3(b). The

TABLE I. Fitting parameters of the sheet resistance of graphene [18].

	C_1 (BL)	C_2 (BL)	C_3 (SiC)	R_0 [Ω]
EMLG	1000	200	0	313
Graphene/Si-N-C/SiC	850	150	0	378
RCG	0	0	5500	2280

resistance was highest at the lowest temperature, decreased with increasing temperature, and then increased at more than 220 K. The resistance increase at high temperatures may correspond to the phonon scattering. However, this increase could not be explained by the phonon scattering in the buffer layer, which is shown by the red curve in the inset in Fig. 3(b). The resistance increase was more drastic, indicating a higher phonon energy for scattering the electrical carrier. Actually, the plots could be perfectly fitted using the SiC surface phonon energy 116 meV as shown by the blue curve. This fact indicates that RCG was located directly on SiC without any buffer layer.

The overall fitting parameters are summarized in Table I. As the example of another interface modification, the parameters for graphene on the Si-N-C interface layer on SiC are also shown [33]. EMLG and graphene on Si-N-C layer had high C_1 and C_2 values and zero C_3 component. However, RCG had zero C_1 and C_2 , and high C_3 component. The C_3 value of 5500 seems very high, but the actual contribution of the SiC surface phonon to the overall resistance value was very small, as shown in Fig. 3(b) (total resistance, R_{LAP} , R_{IP} values of RCG at RT are 2388, 92, 63 Ω). Thus, compared with EMLG, the phonon scattering in RCG was significantly reduced.

The electronic band structures of EMLG and RCG revealed by angle resolved photoemission spectroscopy (ARPES) are shown in Figs. 3(c), 4(a) and 3(d), 4(c), respectively. They are in agreement with the single Dirac cone, which is clear evidence for homogeneous monolayer graphene [34]. It should be noted that the buffer layer does not exhibit the Dirac cone [11]. In EMLG, the Dirac point is located at about 0.40 eV below the Fermi energy, indicating an electron doping of about $1 \times 10^{13} \text{ cm}^{-2}$ [35,36]. The electron doping in EMLG is understood to be a consequence of the spontaneous polarization of the noncentrosymmetric hexagonal SiC substrate and the presence of the buffer layer [37]. On the other hand, in RCG, the Dirac point is above the Fermi energy, and the estimated Dirac energy was at about +0.48 eV, indicating heavy hole doping. It is known that the buffer layer elimination leads to hole doping [37], and so this feature also indicated the lack of the buffer layer. Figure 4 is the wide area ARPES spectrum of (a),(a') EMLG, (b),(b') the buffer layer, and (c),(c') RCG, together with (d) the constant energy map of RCG at E_F , (e) the momentum distribution curve (MDC), and (f) the band structure of graphene. The single Dirac cone of RCG along the K - M - K' line in the reciprocal space indicated the homogeneity of monolayer graphene in both its structural and electronic aspects. The hole concentration roughly estimated from the size of the Fermi surface was about $7.3 \times 10^{13} \text{ cm}^{-2}$. The Fermi velocity was also estimated from the slope of the band dispersion at the Fermi energy, and it was about $1.3 \times 10^6 \text{ m/s}$, which is larger than that of hydrogen-intercalated QFSMLG [35,38].

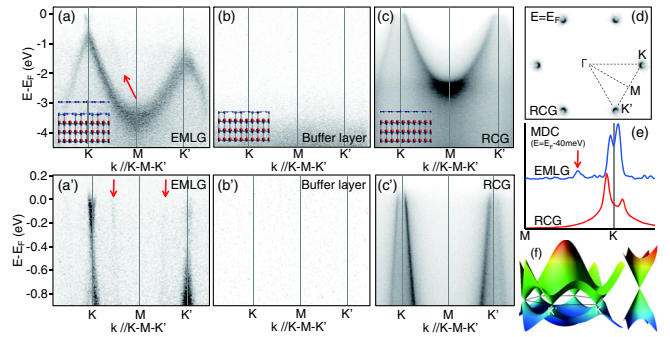


FIG. 4. Wide area ARPES spectra of (a),(a') EMLG, (b),(b') the buffer layer, and (c),(c') RCG. The bands around the K' point are faint because the sample geometry during the measurement was not strictly along the appropriate direction. The constant energy map at the Fermi energy of the RCG sample (d), MDC of EMLG and RCG at $E = E_F - 0.04 \text{ eV}$ (e), and the schematic diagram of the band structure of graphene (f) are also shown.

In addition to the single Dirac cone, there appeared satellite bands in the ARPES spectrum of EMLG, as shown by red arrows in Figs. 4(a),(a') and 4(e) [18]. These satellite bands are induced from the buffer layer [34]. However, Figs. 4(c),(c') and 4(e) show that in RCG, there are no satellite bands. This is another indication of the absence of the buffer layer below RCG.

When the buffer layer is physically converted to monolayer graphene by the RC treatment, the topmost SiC surface has many dangling bonds. In the hydrogen-intercalated QFSMLG, these dangling bonds are satisfied by hydrogen atoms [12]. In order to understand the chemical states of the interface in RCG, we performed x-ray photoelectron spectroscopy (XPS) core level measurements [18]. We can imagine that as RCG was obtained by immersing the buffer layer in the liquid nitrogen, then nitrogen might be intercalated. However, there was no N 1s peak in the RCG sample. Thus, the atomic intercalation is not dominant in the RC effect [18]. At present, we do not have experimental results that directly reveal the state of the Si dangling bonds and the origin of the high hole concentration. One possibility is that a very high amount of Si dangling bonds provides many electrical carriers. This is just one of the hypotheses and further investigation, including theoretical calculation, are needed.

Based on our experimental results, we have found that the buffer layer could be converted to monolayer graphene by the simple and classical RC technique. The RCG thus obtained was high-quality, strain-free, with less phonon scattering, and strongly hole doped. These features induced by the physical decoupling are similar to that of the quasifreestanding graphene produced by hydrogen intercalation. One disadvantage of the hydrogen-intercalated graphene was the lack of thermal stability. By heating at about 1173 K in vacuum, QFSMLG made by hydrogen intercalation was converted back to the buffer layer due to the

hydrogen desorption [11]. In contrast, RCG remained as graphene, even after heating at 1273 K in vacuum, which was demonstrated by the fact that there were no significant changes in the Raman spectrum [18]. It is surprising because of the high reactivity of the Si dangling bonds. However, based on a straightforward analysis from the experimental results, there may be some effect which suppressed the recombination of C and Si. We here speculate the origin. One possibility is that the very small amount of oxygen, which was introduced after rapid-cooling treatment, suppressed the recombination. Another or additional possibility is that C-Si distance was too large, which was observed in a part of TEM images in Fig. S1.

The process of the physical decoupling is simple and does not need any explosive gases nor chemical treatments. In this study, we used a post-growth rapid-cooling technique. The one-time use of the quartz tube is not appropriate for industrial processing. In addition, the small D band in Fig. 2(d) and the large R_0 value in Table I indicate that the RCG has sparse structural defects. These defects are probably due to relatively rough RC treatment and contamination from air during transfer. One alternative idea is the following. Just after we have grown the buffer layer, we can rapidly cool the sample within the chamber by blowing Ar gas onto the sample to transfer it onto a copper plate which is conductively cooled by liquid nitrogen. This process also helps us to avoid the contamination introduced during the transfer between experiments, which would reduce the residual resistance of RCG. Thus, we think it will be a significant contribution to the next generation of high-performance electronic device applications.

This work was supported by the Asahi Glass Foundation and JSPS KAKENHI Grants No. JP25107002 and No. JP26706014, and Natural Science Foundation of Inner Mongolia Autonomous Region of China (No. 2016BS0108).

*To whom all correspondence should be addressed.
w_norimatsu@imass.nagoya-u.ac.jp

†Present address: College of Physics and Electronics Information, Inner Mongolia University for Nationalities, Tongliao 028043, China.

- [1] A. K. Geim and K. S. Novoselov, The rise of graphene, *Nat. Mater.* **6**, 183 (2007).
- [2] C. R. Dean, A. F. Young, I. Meric, C. Lee, L. Wang, S. Sorgenfrei, K. Watanabe, T. Taniguchi, P. Kum, K. L. Shepard, and J. Hone, Boron nitride substrates for high-quality graphene electronics, *Nat. Nanotechnol.* **5**, 722 (2010).
- [3] Y. M. Lin, K. A. Jenkins, A. Valdes-Garcis, J. P. Small, D. B. Farmer, and Ph. Avouris, Operation of graphene transistors at gigahertz frequencies, *Nano Lett.* **9**, 422 (2009).
- [4] C. Berger, Z. Song, X. Li, X. Wu, N. Brown, C. Naud, D. Mayou, T. Li, H. Hass, A. N. Marchenkov, E. H. Conrad, P. N. First, and W. A. de Heer, Electronic confinement and coherence in patterned epitaxial graphene, *Science* **312**, 1191 (2006).
- [5] K. V. Emtsev, A. Bostwick, K. Horn, J. Jobst, G. L. Kellogg, L. Ley, J. L. McChesney, T. Ohta, S. A. Reshanov, J. Rohrl, E. Rotenberg, A. K. Schmid, D. Waldmann, H. B. Weber, and Th. Seyller, Towards wafer-size graphene layers by atmospheric pressure graphitization of silicon carbide, *Nat. Mater.* **8**, 203 (2009).
- [6] W. Norimatsu and M. Kusunoki, Epitaxial graphene on SiC{0001}: Advances and perspectives, *Phys. Chem. Chem. Phys.* **16**, 3501 (2014).
- [7] J. Jobst, D. Waldmann, F. Speck, R. Hirner, D. K. Maude, Th. Seyller, and H. B. Weber, Quantum oscillations and quantum Hall effect in epitaxial graphene, *Phys. Rev. B* **81**, 195434 (2010).
- [8] W. Norimatsu and M. Kusunoki, Transitional structure of the interface between graphene and 6H-SiC (0001), *Chem. Phys. Lett.* **468**, 52 (2009).
- [9] C. Riedl and U. Starke, Structural properties of the graphene-SiC(0001) interface as a key for the preparation of homogeneous large-terrace graphene surfaces, *Phys. Rev. B* **76**, 245406 (2007).
- [10] K. V. Emtsev, F. Speck, Th. Seyller, L. Ley, and J. D. Riley, Interaction, growth, and ordering of epitaxial graphene on SiC{0001} surfaces: A comparative photoelectron spectroscopy study, *Phys. Rev. B* **77**, 155303 (2008).
- [11] C. Riedl, C. Coletti, T. Iwasaki, A. A. Zakharov, and U. Starke, Quasi-Free-Standing Epitaxial Graphene on SiC Obtained by Hydrogen Intercalation, *Phys. Rev. Lett.* **103**, 246804 (2009).
- [12] F. Speck, J. Jobst, F. Fromm, M. Ostler, D. Waldmann, M. Hundhausen, H. B. Weber, and Th. Seyller, The quasi-free-standing nature of graphene on H-saturated SiC(0001), *Appl. Phys. Lett.* **99**, 122106 (2011).
- [13] K. V. Zakharchenko, M. I. Katsnelson, and A. Fasolino, Finite Temperature Lattice Properties of Graphene beyond the Quasiharmonic Approximation, *Phys. Rev. Lett.* **102**, 046808 (2009).
- [14] N. Mounet and N. Marzari, First-principles determination of the structural, vibrational and thermodynamic properties of diamond, graphite, and derivatives, *Phys. Rev. B* **71**, 205214 (2005).
- [15] D. Yoon, Y. W. Son, and H. Cheong, Negative thermal expansion coefficient of graphene measured by Raman spectroscopy, *Nano Lett.* **11**, 3227 (2011).
- [16] W. C. Morgan, Thermal expansion coefficients of graphite crystals, *Carbon* **10**, 73 (1972).
- [17] A. Taylor and R. M. Jones, *Silicon Carbide - A High Temperature Semiconductor*, edited by J. R. O'Connor and J. Smiltens (Pergamon Press, Oxford, 1960), p. 147.
- [18] See Supplemental Material at <http://link.aps.org/supplemental/10.1103/PhysRevLett.117.205501> for the experimental details and additional figures.
- [19] W. Norimatsu and M. Kusunoki, Formation process of graphene on SiC (0001), *Physica E* **42**, 691 (2010).
- [20] W. Norimatsu and M. Kusunoki, Selective formation of ABC-stacked graphene layers on SiC(0001), *Phys. Rev. B* **81**, 161410(R) (2010).
- [21] W. Norimatsu and M. Kusunoki, Structural features of epitaxial graphene on SiC{0001}, *J. Phys. D* **47**, 094017 (2014).

- [22] F. Fromm, M. H. Oliveira, Jr., A. Molina-Sanchez, M. Hundhausen, J. M. J. Lopes, H. Riechrt, L. Wirtz, and Th. Seyller, Contribution of the buffer layer to the Raman spectrum of epitaxial graphene on SiC(0001), *New J. Phys.* **15**, 043031 (2013).
- [23] A. C. Ferrari, J. C. Meyer, V. Scardaci, C. Casiraghi, M. Lazzeri, F. Mauri, S. Piscanec, D. Jiang, K. S. Novoselov, S. Roth, and A. K. Geim, Raman Spectrum of Graphene and Graphene Layers, *Phys. Rev. Lett.* **97**, 187401 (2006).
- [24] J. Röhrl, M. Hundhausen, K. V. Emtsev, Th. Seyller, R. Graupner, and L. Ley, Raman spectra of epitaxial graphene on SiC (0001), *Appl. Phys. Lett.* **92**, 201918 (2008).
- [25] D. S. Lee, C. Riedl, B. Krauss, K. von Klitzing, E. Starke, and J. H. Smet, Raman spectra of epitaxial graphene on SiC and of epitaxial graphene transferred to SiO₂, *Nano Lett.* **8**, 4320 (2008).
- [26] N. Ferralis, R. Maboudian, and C. Carraro, Evidence of Structural Strain in Epitaxial Graphene Layers on 6H-SiC (0001), *Phys. Rev. Lett.* **101**, 156801 (2008).
- [27] J. H. Chen, C. Jang, S. Xiao, M. Ishigami, and M. S. Fuhrer, Intrinsic and Extrinsic performance limits of graphene devices on SiO₂, *Nat. Nanotechnol.* **3**, 206 (2008).
- [28] D. B. Farmer, V. Perebeinos, Y-M. Lin, C. Dimitrakopoulos, and Ph. Avouris, Charge trapping and scattering in epitaxial graphene, *Phys. Rev. B* **84**, 205417 (2011).
- [29] S. Tanabe, Y. Sekine, H. Kageshima, M. Nagase, and H. Hibino, Carrier transport mechanism in graphene on SiC (0001), *Phys. Rev. B* **84**, 115458 (2011).
- [30] A. J. M. Giesbers, P. Prochazka, and C. F. J. Flipse, Surface phonon scattering in epitaxial graphene on 6H-SiC, *Phys. Rev. B* **87**, 195405 (2013).
- [31] C. W. J. Beenakker and H. van Houten, Quantum Transport in Semiconductor Nanostructures, *Solid State Physics* (Academic, New York, 1991), Vol. 44.
- [32] C. Barone, F. Romeo, S. Pagano, C. Attanasio, G. Carapella, C. Cirillo, A. Galdi, G. Grimaldi, A. Guarino, A. Leo, A. Nigro, and P. Sabatino, Nonequilibrium fluctuations as a distinctive feature of weak localization, *Sci. Rep.* **5**, 10705 (2015).
- [33] Y. Masuda, W. Norimatsu, and M. Kusunoki, Formation of a nitride interface in epitaxial graphene on SiC (0001), *Phys. Rev. B* **91**, 075421 (2015).
- [34] A. Bostwick, T. Ohta, Th. Seyller, K. Horn, and E. Rotenberg, Quasiparticle dynamics in graphene, *Nat. Phys.* **3**, 36 (2007).
- [35] C. Riedl, C. Coletti, and U. Starke, Structural and electronic properties of epitaxial graphene on SiC (0001): A review of growth, characterization, transfer doping and hydrogen intercalation, *J. Phys. D* **43**, 374009 (2010).
- [36] M. Kusunoki, W. Norimatsu, J. Bao, K. Morita, and U. Starke, Growth and features of epitaxial graphene on SiC, *J. Phys. Soc. Jpn.* **84**, 121014 (2015).
- [37] J. Ristein, S. Mammadov, and Th. Seyller, Origin of Doping in Quasi-Free-Standing Graphene on Silicon Carbide, *Phys. Rev. Lett.* **108**, 246104 (2012).
- [38] D. A. Siegel, C-H. Park, C. Hwang, J. Deslippe, A. V. Fedorov, S. G. Louie, and A. Lanzara, Many-body interactions in quasi-freestanding graphene, *Proc. Natl. Acad. Sci. U.S.A.* **108**, 11365 (2011).